

This is a repository copy of *Piezoelectric-resonator-based power supply for an ozone-generating dielectric barrier discharge reactor*.

White Rose Research Online URL for this paper: https://eprints.whiterose.ac.uk/id/eprint/233130/

Version: Accepted Version

Article:

O'Keeffe, H. orcid.org/0009-0008-5559-9862, Foster, M.P. orcid.org/0000-0002-8565-0541 and Davidson, J.N. orcid.org/0000-0002-6576-3995 (2025) Piezoelectric-resonator-based power supply for an ozone-generating dielectric barrier discharge reactor. IEEE Transactions on Plasma Science, 53 (10). pp. 3105-3112. ISSN: 0093-3813

https://doi.org/10.1109/tps.2025.3598886

© 2025 The Authors. Except as otherwise noted, this author-accepted version of a journal article published in IEEE Transactions on Plasma Science is made available via the University of Sheffield Research Publications and Copyright Policy under the terms of the Creative Commons Attribution 4.0 International License (CC-BY 4.0), which permits unrestricted use, distribution and reproduction in any medium, provided the original work is properly cited. To view a copy of this licence, visit http://creativecommons.org/licenses/by/4.0/

Reuse

This article is distributed under the terms of the Creative Commons Attribution (CC BY) licence. This licence allows you to distribute, remix, tweak, and build upon the work, even commercially, as long as you credit the authors for the original work. More information and the full terms of the licence here: https://creativecommons.org/licenses/

Takedown

If you consider content in White Rose Research Online to be in breach of UK law, please notify us by emailing eprints@whiterose.ac.uk including the URL of the record and the reason for the withdrawal request.



Piezoelectric Resonator Based Power Supply for an Ozone-Generating Dielectric Barrier Discharge Reactor

Henry O'Keeffe, Martin P. Foster, Jonathan N. Davidson

Abstract—In this work, a dielectric barrier discharge (DBD) reactor power supply designed for operation with a low input voltage is presented. A piezoelectric resonator is used to provide voltage gain and high efficiency in a small volume for portable (point of use) ozone generation, suitable for the disinfection of surfaces for example. The power supply was coupled to a small, asymmetrical DBD reactor and achieved an efficiency of 63% and an ozone generation efficacy of 67 g/kWh when operating at 4.4 W. The use of a piezoelectric resonator (PR) to provide voltage gain has several advantages over, for example, a traditional electromagnetic transformer. The PR has monolithic construction for reliability, is inherently insulated against high voltage due to the ceramic material, can operate up to 300°C, and its resonant behaviour allows the power supply to operate with zero-voltage switching.

Index Terms—Resonant Converter, Dielectric Barrier Discharge, Piezoelectrics, Ozoniser

I. INTRODUCTION

ZONE (O₃) is a reactive chemical species of oxygen formed from three oxygen atoms [1]. Ozone breaks down to form short-lived oxygen radicals which readily combine with organic compounds, altering their composition. This has led to applications in toxic-gas treatment [2], medicine [1], water filtration [2], [3], and many others where ozone's ability to destroy organic compounds can be utilised [2]. Ozone is currently most efficiently produced in a dielectric barrier discharge (DBD) reactor [4].

A. Dielectric Barrier Discharge Reactors

DBD reactors are a category of chemical reactors that can produce high-value chemicals on a small scale. They are also suitable for low-cost ozone production with a modular design and are known as ozonisers in this role. They provide an opportunity for small-scale testing (such as in lab-on-a-chip systems) and allow the use of renewable energy for chemical production as they derive the activation energy from electricity. A significant challenge in their design is the high-voltage (HV) power supply required to produce high electric fields >1 kV/mm. The structure of a DBD reactor (Fig. 1) usually consists of a pair of electrodes with one or more insulating layers between them, with at least one of the layers being a dielectric (e.g., glass, quartz or ceramic) and one of the

Date submitted for review: ____ This work has been financially supported by The Engineering and Physical Sciences Research Council: EP/S031421/1. (Corresponding author: Henry O'Keeffe).

The authors are with the Department of Electrical and Electronic Engineering, University of Sheffield, S1 3JD, Sheffield, UK.

(email: hokeeffe1@sheffield.ac.uk; m.p.foster@sheffield.ac.uk; jonathan.davidson@sheffield.ac.uk)

electrodes exposed to gas (air or oxygen for ozone generation).

A reactor can either be symmetrical (electrodes of the same type) or asymmetrical (electrodes of differing types e.g., one conductive, and one with a dielectric coating).

In this work, an alumina (aluminium oxide) coating on an aluminium electrode (labelled A in Fig. 1) forms the dielectric and brass is used for the second electrode (labelled B).

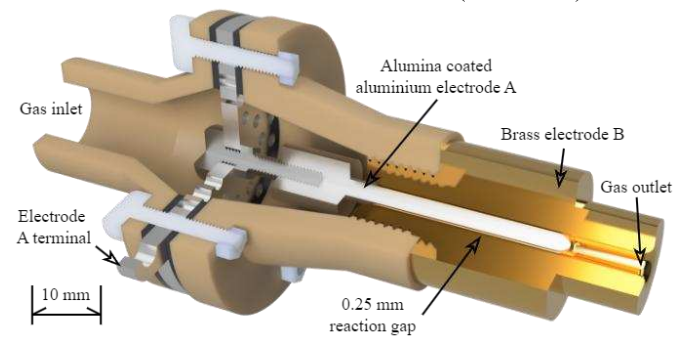


Fig. 1. Cut-away 3D model of the DBD reactor

An HV bipolar waveform is applied to the electrodes, causing a small current to flow through the reactor due to its capacitance. A charge builds up on the surface of the dielectric until the potential difference across the gap adjacent to the charge carrier exceeds the breakdown voltage of the gas in the gap, causing localised discharge (streamers) through the gas. Each streamer exists for tens of nanoseconds.

This discharge reduces the charge on the dielectric to the point the voltage across the gap can no longer support further discharge. The current flowing though the largely capacitive reactor causes charge to build up again until another discharge occurs. Compared to continuous discharge, this cycle of charge and discharge limits the energy supplied to the gas and the resultant plasma. This type of plasma is known as non-thermal, or "cold" plasma and is favourable for ozone generation, as it prevents high temperature from prematurely breaking down any ozone formed.

The electrical input to a DBD reactor must, therefore, have sufficient voltage to cause breakdown of the gas in the gap, i.e. it must be greater than the ignition voltage, and must be bipolar to allow current flow to reset the charge on the dielectric. The input voltage and frequency of continuous-wave DBD reactors vary over a wide range depending on design requirements. The parameters of some examples from literature are shown in Table I, showing that peak operating voltages range from 700 V to 6 kV, frequency ranges from 5 kHz to 57.5 kHz over power ranges of 0.15 W to 240 W.

	TABLE I
DBD OZONISER PARAMETERS FROM LITERATURI	DBD OZONISER PARAMETERS FROM LITERATURE

Ref	Voltage (kVpk)	Frequency (kHz)	Power (W)	PSU efficiency (%)	Ozoniser efficacy (g/kWh)
[4]	3–6	25	12-53*	-	-
[5]	2.3-4.3	19	32-1015	≤ 81	-
[6]	2.4–3	26.3	0.3-3	-	≤ 140 (air) ≤ 223 (O ₂)
[7]	0.8 - 1.25	53.4	1.4-4	90	$\leq 3.4 \; (O_2)$
[8]	5	5*	0.15-1	-	$\leq 206 \text{ (air)}$ $\leq 414 \text{ (O}_2)$
[9]	3.44	45-57.5	9-40	30-85	4.5-21
[10]	0.7	15.6	1	50	6 (O ₂)
This Work	0.9-1.1	~56.9	0.5-4.5	63	45-105 (air)

* subject to caveat explained in the reference

B. DBD Reactor Modelling

DBD reactors are commonly electrically modelled as a pair of series capacitors with a switch and resistor connected in parallel with one of them [11], seen in Fig. 2a, where C_B is the bulk capacitance of the reactor, C_G is the capacitance of the discharge gap and R_G models the discharge. For a period of each cycle, Sw is closed, representing the occurrence of discharge, thereby extracting energy from the system.

In [12], Alonso, et al. simplified the model of the DBD reactor to the parallel RC network shown in Fig. 2b, allowing it to be used in linear systems. In addition, a reactor with an input voltage lower than the ignition voltage can be modelled as purely capacitive [13].

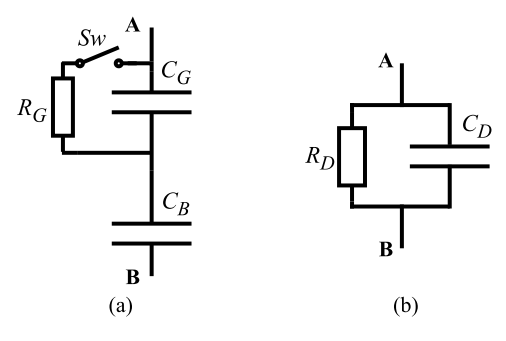


Fig. 2. (a) Conventional DBD reactor model and (b) high-frequency DBD reactor model

The plasma discharges cause significant stochastic electrical noise: both radiating EMI and creating noise on the input current waveform, although this is not modelled in either the conventional DBD reactor model or the high-frequency model.

C. DBD Reactor Power Supply

Power supply topologies used for DBD include the resonant LLCC half-bridge [14], a transformer-coupled LC resonant H-bridge [15] and the phase-shifted full bridge [9] amongst others. As with other types of power supply, resonance allows high efficiency and, in this application, results in a sinusoidal output voltage with low harmonic distortion.

As DBD reactor power is proportional to the frequency of the reactor input waveform [2], a higher frequency power supply can be used to obtain a higher production rate in an ozone-generating reactor, for example. For small, portable DBD reactors, a simple topology such as the single-switch resonant flyback converter presented in [10] can be used, although the topology has only been demonstrated with 50% efficiency.

In [5], a resonant series-parallel converter is presented where a series LC tank drives a parallel LC tank and achieves zero-current switching (ZCS). This topology is transformer-coupled, with the transformer accounting for a large part of the total losses and system volume.

Alternatively, a piezoelectric transformer (PT) can provide voltage gain and isolation while also forming the resonant tank. PTs are three- or four-terminal devices that use the piezoelectric effect at or near resonance. An alternating voltage is applied between the input electrodes and a higher or lower voltage is induced between the output electrodes.

PTs have been used to provide voltage gain for driving low-power DBD reactors in the literature. In [7], Salam et al. report 90% power supply efficiency for a 4 W reactor, resulting in 3.6 g/kWh of ozone production with pure oxygen as the feedstock.

Due to the capacitance of the PT, any driving circuit usually has a series inductor to reduce switching losses. This inductor adds size and weight to the system and represents a source of additional power loss.

D. Piezoelectric Resonators

Piezoelectric devices use the electromechanical properties of a piezoelectric material to convert electrical energy to mechanical energy and vice versa. Such devices exploit mechanical resonance whose natural frequency is dependent on the material parameters and geometry.

There are two piezoelectric devices commonly used in power electronics: the two-port piezoelectric transformer (PT) and the one-port piezoelectric resonator (PR).

Whilst the piezoelectric transformer has been studied for DBD reactor power supply applications ([6], [16], [17], [18]), this paper is the first to study the use of a PR for reactor power supply design. A PR is a simpler device than a PT; only having one-port, it cannot provide voltage gain without additional components. As in the PT, an external voltage applied to the PR causes the material to deform. Mechanical resonance, coupled to the electrical domain by the piezoelectric properties of the material, allows it to be electrically modelled with the Van Dyke equivalent circuit shown in Fig. 3 [19], [20].

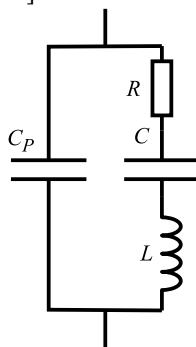


Fig. 3. Van Dyke equivalent circuit model of a piezoelectric resonator

Due to the properties of the piezoelectric material, a high Q-factor of over 600 can be achieved for a lead zirconate titanate (PZT) resonator [20]. This makes the equivalent circuit unrealisable with electrical components in a volume comparable to the resonator. For example, a PZT resonator with a volume of 11.87 mm³, which has parameters $R = 4.45 \ \Omega$, $C = 75.2 \ pF$, and $L = 1.51 \ mH$, is used in the DC-DC converter described in [21].

This paper describes the use of a piezoelectric resonator in a high-voltage power supply, for use with a DBD reactor. The high Q-factor of the piezoelectric resonator reacts with an external capacitance to achieve the required voltage gain necessary to initiate discharge.

II. PARAMETERISATION

A. Parameterisation of the DBD reactor

To design the power supply, accurate equivalent component values must be determined for the electrical equivalent models for the reactor and PR.

The DBD reactor used here is a co-axial type with an alumina-coated inner (A) electrode. The key dimensions and parameters can be seen in Table II. The design can be seen in Fig. 1.

TABLE II
DBD REACTOR DIMENSIONS AND PARAMETERS

Inner electrode diameter	3 mm
Alumina dielectric thickness	$\sim 60~\mu m$
Average electrode gap distance	0.25 mm
Electrode active length	20 mm
Reactor frequency test range	10 - 85 kHz
Reactor voltage test range	$582 - 886 V_{RMS}$
Maximum reactor power	5 W

The reactor was tested with the characterisation set-up shown in Fig. 4 using the Lissajous method [8] where C_S is the current-sense capacitor. These tests were performed over the range of operating frequencies and voltages given in Table II to find values of R_D (shown in Fig. 2). To reduce degradation of the electrode the power was limited to 5 W.

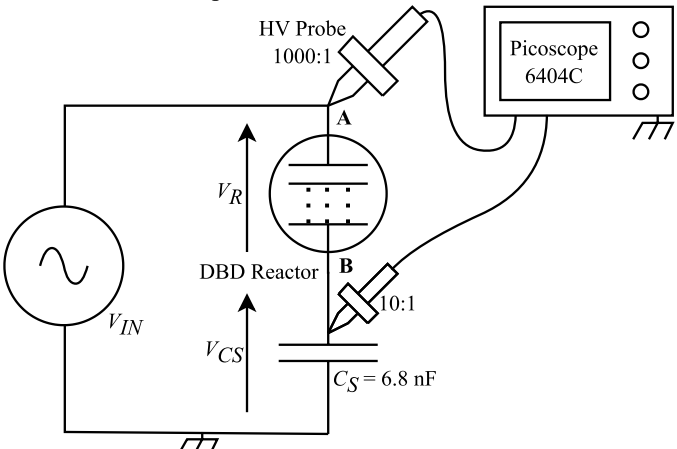


Fig. 4. DBD reactor characterisation setup

A Picoscope 6404C, TREK 10/40A-HS HV amplifier, Tektronix P6015A HV probe, and RSDG 830 waveform generator were used for these tests.

The waveforms taken were used to calculate average power dissipated in the reactor with (1). This was then used with the RMS reactor voltage to calculate the R_D for each voltage and frequency.

$$P_{av} = \frac{C_S}{T_{av}} \int_{t=0}^{t=T_{av}} V_R(t) \, dV_{CS}(t) \tag{1}$$

Where $T_{\rm av} \gg 1/f$, f is the frequency of the sinusoidal reactor voltage, $V_{\rm R}$ and $V_{\rm CS}$ is the voltage across the sense capacitor $C_{\rm S}$

Whilst the capacitance of the reactor can be calculated from its geometry, in practice there will be additional parasitic capacitance from the other parts of the reactor such as wiring.

To provide an accurate estimate of $C_{\rm D}$, the effective capacitance of the reactor, $C_{\rm R}$, was calculated from the characterisation test data using (2) with a $V_{\rm IN}$ lower than the ignition threshold (500 $V_{\rm pk}$) and was found to be 11.4 pF.

$$C_{\rm D} = \frac{C_{\rm S} V_{\rm CS}}{V_{\rm R}} \tag{2}$$

Whilst in operation, charge accumulates in the reaction gap, (as highlighted in Fig. 1). This causes the capacitance to change under load. Other authors [9], [10], [12] have found that this change is typically <20%, depending on the type of reactor, whilst $R_{\rm D}$ can vary significantly with reactor output power. To account for this variation, an expression for $R_{\rm D}$ as a function of frequency and reactor input voltage was found. Thus (3) was fitted to the data from these tests using a mean-square-percentage-error cost function, (4), and a particle swarm optimiser to ensure a global best fit was found.

$$R_{\rm D} = \frac{aV_R^b}{f} \tag{3}$$

where a and b are constants chosen by the fitting algorithm which minimises the mean square error (E_{MS}).

$$E_{\rm MS} = \frac{\sum_{k=1}^{N} \left(\frac{M_k - F_k}{M_k}\right)^2}{N} \tag{4}$$

where N is the number of data points used in the fit, M is the measured data, and F is the data from the equation being fitted. The curve fit can be seen in Fig. 5. The constants were determined to be $a = 1.0 \times 10^{26} \,\Omega$.Hz.V^{5.52} and b = -5.52.

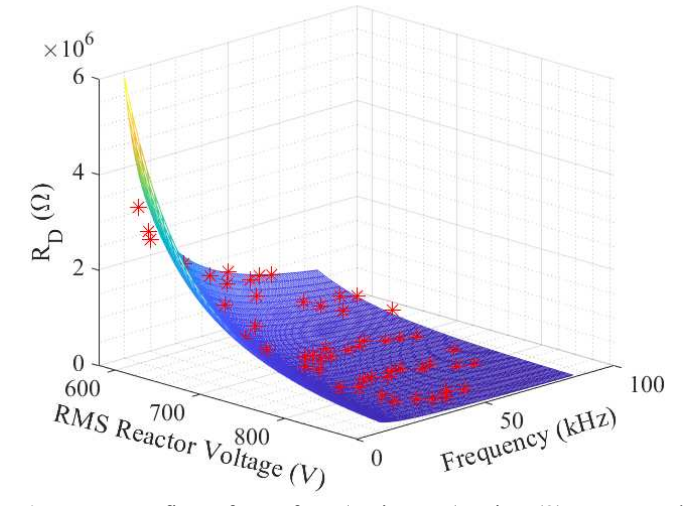


Fig. 5. Curve fit surface of R_D (resistance) using (3). Measured data points are indicated with red stars.

B. Parameterisation of the piezoelectric resonators

In [22] a particle swarm optimisation method was described for finding the input impedance of a piezoelectric transformer. This technique was adapted to determine the first resonant mode of three PRs from STEMiNC; the parameters are shown in Table III. An example of the closeness of the fit is in Fig. 6.

TABLE III PIEZOELECTRIC RESONATOR PARAMETERS

	SMD25T85F234S	SMD35T12S118	SMD43T105F200S
$C_{\rm P}\left({\rm pF}\right)$	494	567	1140
$R(\Omega)$	13.5	10.7	4.31
L (mH)	17.5	33.4	20.2
C(pF)	194	188	508
$Q_{ m RLC}$	704	1250	1460

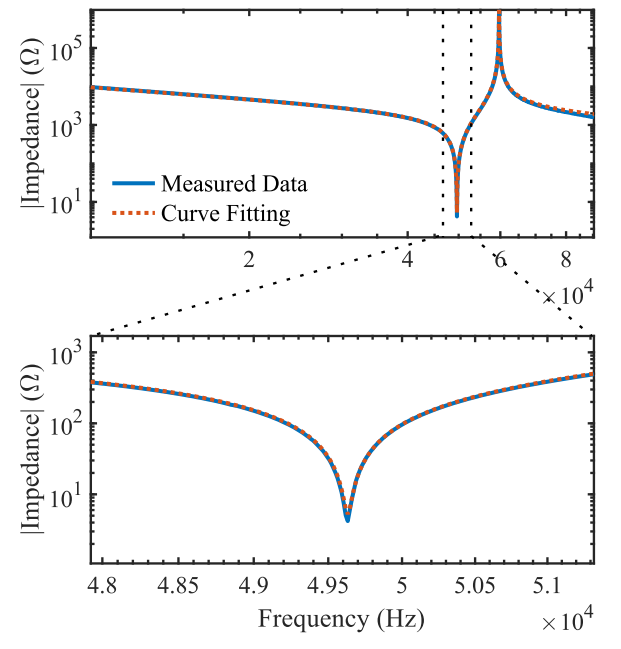


Fig. 6. Resonator parameterisation fit to measured data for the SMD43T105F200S.

III. VOLTAGE GAIN

Without the inherent voltage gain of a transformer, the suitability of a piezoelectric resonator for generating high voltages for a DBD reactor is not immediately apparent. In this work, the RLC branch in the Van Dyke model is made to resonate with a parallel combination of the reactor capacitance, C_R , and a discrete capacitor, C_A . C_A is tuned to maximise the gain of the system, although this does not necessarily maximise its efficiency. The total capacitance seen by the Van Dyke model (Fig. 7) is $C_D = C_R + C_A$.

The complex frequency domain equation for the gain of the circuit in Fig. 7 is shown in (5).

$$\frac{V_R}{V_I} = \frac{s^3 R_D L C_P C + s^2 R R_D C_P C + s R_D (C_P + C)}{s^3 C L R_D (C_D + C_P) + s^2 C (C_D R_D R + C_P R_D R + L) + s (R_D C_D + C_P R_D + C R_D + R C) + 1} (5)$$
where the complex frequency, $s = j\omega$, j is the imaginary unit and ω is angular frequency.

To calculate the frequency at which the maximum gain occurs, (3) was substituted into (5) to eliminate $R_D(V_R)$, and a least-squares optimiser varied the frequency, ω , to maximise V_R for a given $V_I = 48 \ V_{pk}$.

Output power, P_0 , is defined as the power dissipated by the linear-model load resistance (Fig. 2), R_D ,

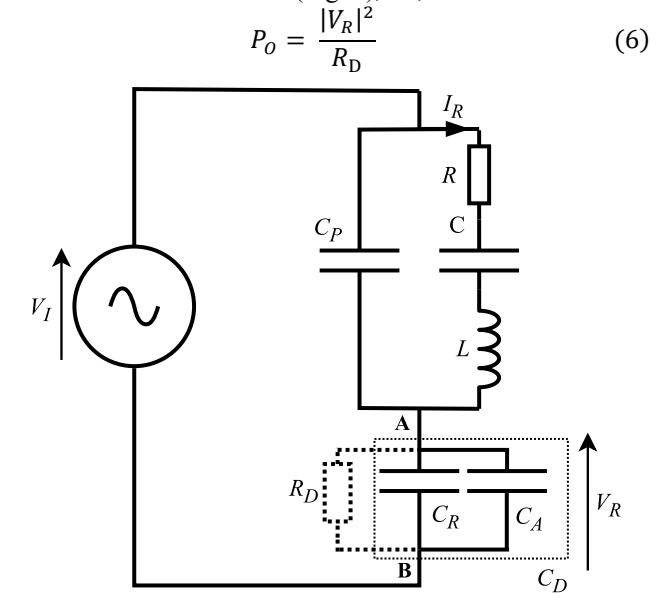


Fig. 7. Proposed power supply circuit diagram showing the PR Van Dyke model with AC voltage source, series capacitance (C_A) and DBD reactor model $(C_R & R_D)$.

The only other source of power dissipation in Fig. 7 is the resistance in the model of the PR, R. The power dissipated in this resistor is given by,

$$P_R = |I_R|^2 R \tag{7}$$
was formulated in terms of V

 I_R was formulated in terms of V_I ,

$$\frac{s_{V_{I}C}(s_{R_{D}}C_{D}+1)}{1+s^{3}CLR_{D}(c_{D}+C_{P})+s^{2}C(R(c_{D}+C_{P})R_{D}+L)+s((c+c_{D}+C_{P})R_{D}+CR)}$$
(8)

where C, R, etc. are shown in Fig. 7. The efficiency, η , can then be calculated from P_O and P_R ,

$$\eta = \frac{P_0}{P_0 + P_R} \tag{9}$$

These calculations were performed for each resonator with a range of C_D to analyse the effects of C_D on output power and efficiency. These results can be seen in Fig. 8.

Comparion of the results for the three PRs in Fig. 8 shows that the largest resonator, SMD43T105F200S with the highest Q-factor and lowest impedance at resonance (seen in Table III) exhibits a higher maximum power and higher efficiency than the other two resonators. For this reason, this resonator was chosen for the final design.

As the power rating of the reactor is 5 W (Table II), the power supply can be designed for this power, maximising efficiency because the efficiency and power have an inverse relationship as $C_{\rm D}$ is increased (Fig. 8a and Fig. 8b respectively). 5 W corresponds to a $C_{\rm D}$ of ~500 pF, an efficiency of 88% and frequency of 56.7 kHz. $C_{\rm A}$ was chosen to be 500 pF as $C_{\rm R}$ is negligible for this reactor.

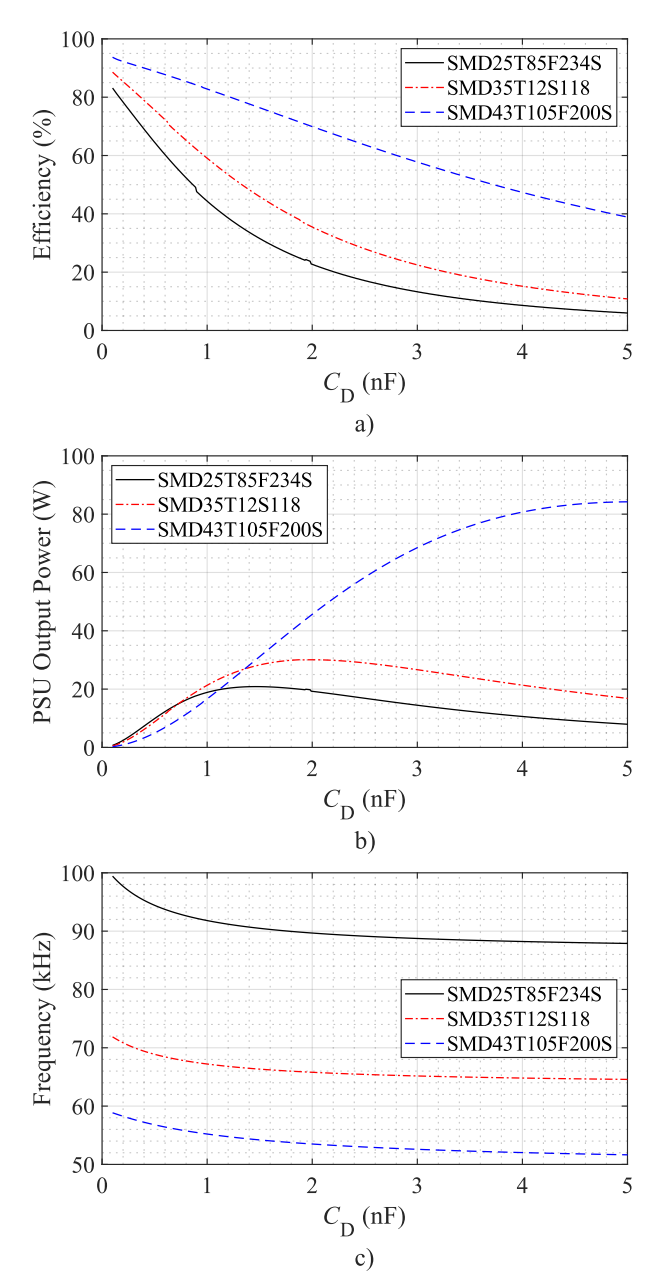


Fig. 8. Simulated effect of C_D on a) efficiency, b) maximum power and c) frequency for the three resonators in Table III

IV. LOW VOLTAGE AC SUPPLY

To drive this system, any voltage source with an AC component can be used: any DC voltage component will be blocked by the resonator and only spectral components around the resonant frequency will contribute significantly to the reactor power.

A GaN full-bridge inverter was used as the AC supply for this system. The specifications can be seen in Table IV. A half-bridge can alternatively be used but has half the output voltage of a full bridge. The half bridge is generally cheaper but requires higher resonant system gain, reducing overall system efficiency.

To reduce the switching losses associated with switching a capacitive load, a deadtime of 10% was used. The deadtime allows energy to be recovered from the PR acoustic wave to charge the capacitance on the output of the inverter during this dead time.

TABLE IV
INVERTER SPECIFICATIONS

Bus voltage	48 V
GaN switches	TI LMG5200
Controller IC	dsPIC33CH512MP505
Switch on-state resistance	15 mΩ
Switch slew-rate	50 V/ns
Switch current rating	10 A
PCB dimensions	$55 \text{ mm} \times 32 \text{ mm}$

V. EXPERIMENTAL RESULTS

The experimental setup can be seen in Fig. 9. The additional equipment used over previous tests was a Yokogawa PX8000 power analyser to assess the performance of the inverter, and a 48 V DC supply to power the system. The connection of this test equipment necessitated wires approximately 50 cm in length. These have a parasitic inductance on the order of microhenries represented by L_P in Fig. 9.

The PX8000 was used to measure the voltage and current at the input and output of the inverter ($V_{\rm DC}$, $I_{\rm DC}$, $V_{\rm IV}$, $I_{\rm IV}$). Fig. 10a shows the waveforms of the inverter output current and voltage when operating with an output power of 0.4 W. The 10% deadtime allows the resonant current (leading the voltage by approximately 90°) to charge the capacitance present on the output of the inverter, causing the inverter output current to

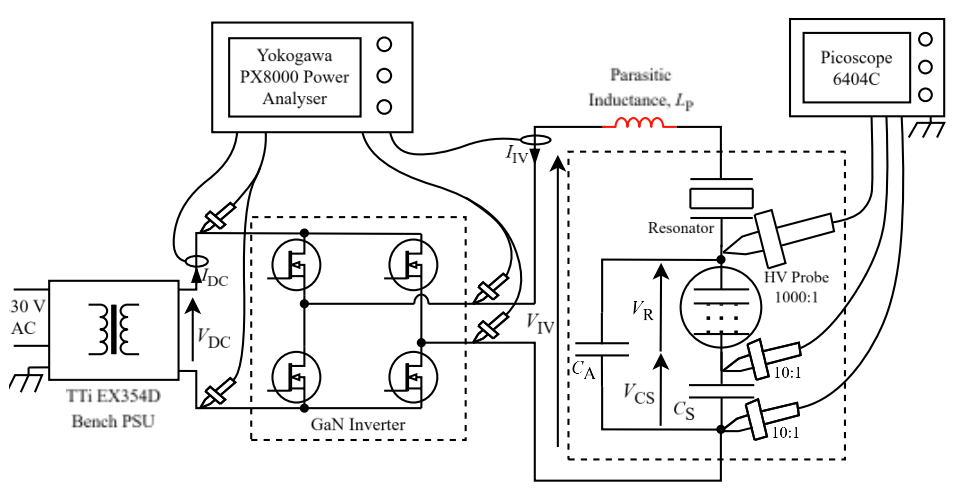


Fig. 9. Experimental test set-up

drop and the output voltage to rise to the bus voltage during the deadtime, achieving ZVS. Also visible is a high frequency component: ringing resulting from the change in current (0.2 A) through the resonator and parasitic inductance (L_P) in a short period of time (100 ns).

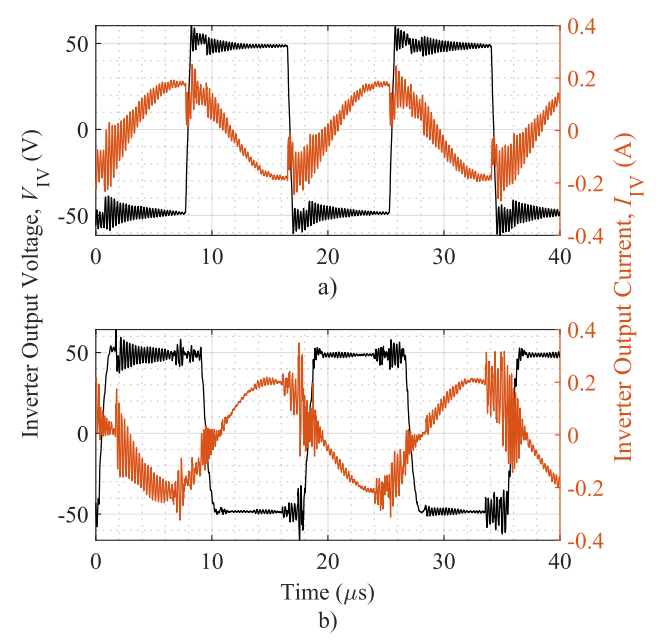


Fig. 10. Inverter waveforms, a) $P_0 = 0.4 \text{ W}$, b) $P_0 = 4.4 \text{ W}$.

Fig. 10b shows these waveforms during operation at $P_{\rm O}=4.4~\rm W$. The voltage-leading phase shift has now increased to 150° and there is less current available during the deadtime to charge $C_{\rm P}$. By the end of the deadtime, $C_{\rm P}$ has charged with $V_{\rm IV}$ nearly at $V_{\rm DC}$ as the output current crosses 0 at 19 μs . This operating condition represents a limit to the maximum output power of the system whilst still maintaining ZVS.

At 4.4 W there is significant discharge in the reactor. This causes noise on the current and voltage waveforms in Fig. 10b, seen periodically before commutation at 16 μ s for example. There is also generally less ringing at this power level as the reactor current is lower during commutation, resulting in a lower dI_{IV}/dt .

Fig. 11 shows the voltage waveforms on the reactor, V_R , and the current sense capacitor, V_{CS} . These signals are digitally low-pass filtered in post-processing with a corner frequency of 12.5 MHz and attenuation of 60 dB in the cut-off region to reduce high-frequency noise caused by the discharge in the reactor.

 $V_{\rm R}$ is sinusoidal, with a small distortion twice per cycle during the dead time. $V_{\rm CS}$ shows noise from the discharge, visible as many regions of high ${\rm d}V/{\rm d}t$. When one plasma streamer is formed, the resulting conducting channel often prompts nearby charged regions to discharge, resulting in a cascade effect. As these discharges are very short (~10 ns) in duration, this cascade is also very short. This results in a large ΔV_{CS} over a short time, seen at 30 µs in Fig. 11a, for example.

Fig. 11 shows a DC offset on $V_{\rm CS}$. Since the reactor electrodes are asymmetrical, the DC offset is thought to be due to charge build-up on the dielectric. To test this hypothesis,

two pairs of electrodes were used: a pair of identical aluminacoated electrodes as described in Table II, and a set of one coated and one uncoated electrode.

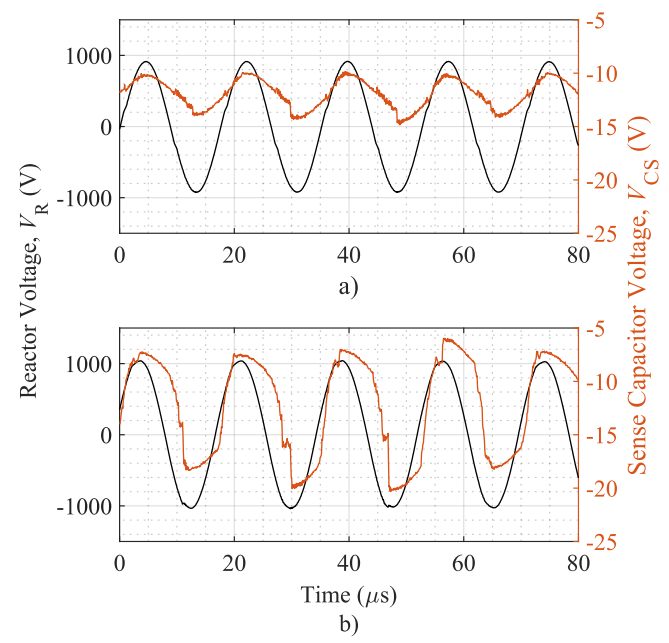


Fig. 11. Reactor waveforms, a) $P_O = 0.4 \text{ W}$, b) $P_O = 4.4 \text{ W}$.

A sinusoidal voltage of approximately 600 V_{pk} at 20 kHz was applied to the electrodes, and the DC offset of V_{CS} was measured over 40 cycles. The pair of identical electrodes (symmetrical) had a DC offset voltage of -0.022 V, whilst the coated / uncoated set (asymmetrical) had a DC offset of 0.2 V, approximately ten times higher than the symmetrical test.

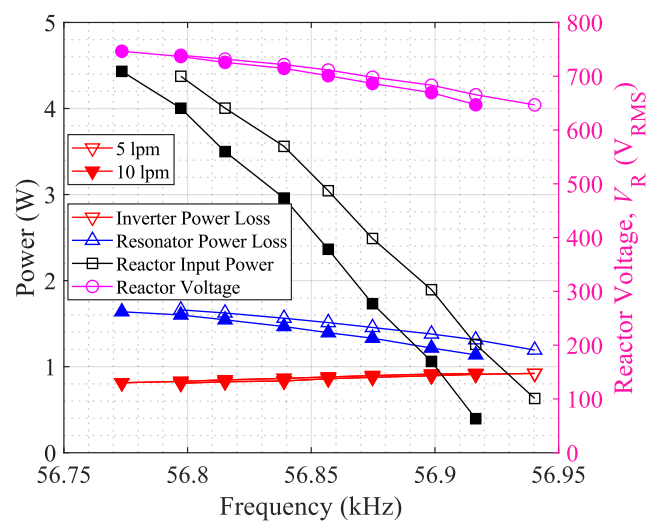


Fig. 12. Reactor voltage and power distribution as frequency is varied.

Fig. 12 shows the variation in power and voltage over the frequency range 56.75 kHz to 56.95 kHz. This is sufficient to change the reactor input power approximately linearly from 0.4 W to 4.4 W, with reactor voltage also varying approximately linearly over the range 647 V_{RMS} to 746 V_{RMS} . This allows the reactor power to be inferred from the reactor voltage.

The change in power and voltage for a given frequency when the flowrate is increased from 5 to 10 litres per minute (lpm) is seen in Fig. 12. This change suggests that parameters in the electrical model of the reactor, C_R and R_D , change with flowrate, perhaps due to the increased flow causing individual discharges to be extinguished faster.

The power loss distribution in Fig. 12 shows the power loss in the inverter reduces as frequency decreases and power increases. The power loss in the resonator increases with reactor power more slowly than the reactor power, meaning efficiency is increasing with reactor power. The system reaches a total efficiency of 63%, with all support circuity (microcontroller, etc.) included in the inverter losses. Considering the resonator alone, the efficiency is 72%. For a given resonator and reactor, this efficiency could be increased at the cost of maximum output power, by reducing C_D (shown in Fig. 8). In future work, improvements could also be made by optimising the design of the reactor and resonator geometry specifically for use in this circuit.

Fig. 13 shows the performance of the DBD reactor. The tests at 10 lpm in had increased efficacy (a ratio of the generated mass of ozone and the energy delivered to the reactor), and a lower ozone concentration probably due to the greater flow also reducing reactor temperatures. The results demonstrate that the reactor is most efficacious at a lower power. This is most likely due to the reduced heating causing less ozone to be destroyed after it is produced as ozone is destroyed at higher temperatures [23].

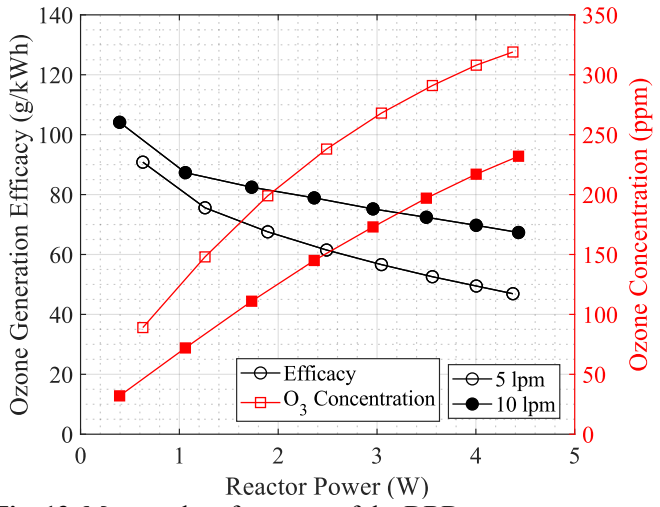


Fig. 13. Measured performance of the DBD reactor.

The system's overall efficiency has a positive trend with reactor power and ozone production, reaching a peak efficiency at the maximum power rating of the reactor, suggesting that this efficiency could be improved further at the expense of a loss of ZVS (as most of the input power is delivered to the reactor, it is likely that despite the reduced efficiency of the inverter, the overall efficacy would increase in line with the reactor efficacy trend).

VI. CONCLUSION

This paper describes the first use of a PR as a device for driving a dielectric barrier discharge. The use of a PR as an energy converter offers several advantages over conventional power supplies, including high efficiency and the ability to operate at high frequencies for increased ozone production. The results show that the power supply achieves 63% efficiency with a reactor voltage of over 740 V_{RMS} at 56.8 kHz. These are shown in Table I. Whilst the efficacy was high, at 67 g/kWh when operating at 4.4 W, further research focused on optimising the efficacy of the reactor could help improve this.

The voltage and power vary linearly with frequency, simplifying control, whilst the reactor is most effective at lower power levels due to reduced heating and a smaller percentage of ozone being destroyed after it is produced. The results demonstrate the potential of the PR-based power supply as a viable alternative to conventional power supplies for DBD reactors.

ACKNOWLEDGEMENT

For the purpose of open access, the authors have applied the creative commons attribution (CC-BY) licence to any author-accepted manuscript arising.

REFERENCES

- [1] S. Maftuhah, A. Rahardian, M. Masfufah, E. Yulianto, S. Sumariyah, and M. Nur, 'Experimental Study on Medical Ozone Generation in Double Dielectric Barrier Discharge (DDBD) with Spiral-Spiral Electrodes', in *Proceedings of 2nd International Conference on Chemical Process and Product Engineering*, Semarang, Indonesia, 2019.
- [2] U. Kogelschatz, 'Dielectric-barrier Discharges: Their History, Discharge Physics, and Industrial Applications', *Plasma Chem. Plasma Process.*, vol. 23, no. 1, pp. 1–46, 2003.
- [3] A. Hafeez, N. Shezad, F. Javed, T. Fazal, M. S. Rehman, and F. Rehman, 'Developing multiplexed plasma micro-reactor for ozone intensification and wastewater treatment', *Chem. Eng. Process. Process Intensif.*, vol. 162, p. 108337, 2021.
- [4] K. Nassour, M. Brahami, S. Nemmich, N. Hammadi, N. Zouzou, and A. Tilmatine, 'Comparative Experimental Study between Surface and Volume DBD Ozone Generator', *Ozone Sci. Eng.*, vol. 38, no. 1, pp. 70–76, 2016.
- [5] T. Jakubowski, M. Holub, and S. Kalisiak, 'Resonant inverter with resonance frequency tracking for DBD plasma reactor supply', *Eur. Phys. J. Appl. Phys.*, vol. 61, no. 2, p. 24304, Feb. 2013, doi: 10.1051/epjap/2012120430.
- [6] K. Teranishi, S. Suzuki, and H. Itoh, 'A novel generation method of dielectric barrier discharge and ozone production using a piezoelectric transformer', *Jpn. J. Appl. Phys.*, vol. 43, no. 9 B, pp. 6733–6739, 2004, doi: 10.1143/JJAP.43.6733.
- [7] Z. Salam, M. Facta, and M. Amjad, 'Design and implementation of a highly efficient DBD ozonizer using the single switch resonant converter with piezoelectric transformer', in 2013 Twenty-Eighth Annual IEEE Applied Power Electronics Conference

- *and Exposition (APEC)*, Mar. 2013, pp. 1596–1600. doi: 10.1109/APEC.2013.6520510.
- [8] T. Homola, V. Prukner, P. Hoffer, and M. Šimek, 'Multi-hollow surface dielectric barrier discharge: an ozone generator with flexible performance and supreme efficiency', *Plasma Sources Sci. Technol.*, vol. 29, no. 9, p. 95014, 2020, doi: 10.1088/1361-6595/aba987.
- [9] P. Hothongkham and V. Kinnares, 'High-voltage high-frequency power supply using a phase-shifted PWM full bridge inverter fed ozone generator with constant applied electrode voltage', in *The 2010 International Power Electronics Conference ECCE ASIA*, Sapporo, Japan, 2010.
- [10] J. Alonso, J. Cardesin, E. Corominas, M. Rico-Secades, and J. Garcia, 'Low-power high-voltage high-frequency power supply for ozone generation', *IEEE Trans. Ind. Appl.*, vol. 40, no. 2, pp. 414–421, 2004.
- [11] H. Jakob and M. Kim, 'Electrical Model for Complex Surface DBD Plasma Sources', *IEEE Trans. Plasma Sci.*, vol. 49, no. 10, pp. 3051–3058, 2021, doi: 10.1109/TPS.2021.3110437.
- [12] J. M. Alonso, M. Valdés, A. J. Calleja, J. Ribas, and J. Losada, 'High Frequency Testing and Modeling of Silent Discharge Ozone Generators', *Ozone Sci. Eng.*, vol. 25, no. 5, pp. 363–376, 2003, doi: 10.1080/01919510390481685.
- [13] M. Ponce, J. Aguilar, J. Fernandez, E. Beutelspacher, J. M. Calderon, and C. Cortes, 'Linear and non linear models for ozone generators considering electrodes losses', in 2004 IEEE 35th Annual Power Electronics Specialists Conference, Piscataway NJ: IEEE, 2004, pp. 810-814 Vol.1. doi: 10.1109/PESC.2004.1355853.
- [14] M. Meisser, M. Paravia, W. Heering, and R. Kling, 'Resonance behaviour of a pulsed electronic control gear for dielectric barrier discharges', in 5th IET International Conference on Power Electronics, Machines and Drives (PEMD 2010, 2010.
- [15] G. Udhayakumar, M. R. Rashmi, K. Patel, G. P. Ramesh, and A. Suresh, 'Implementation of high-frequency high-voltage power supply for ozone generator system using embedded controller', in 2016 International Conference on Circuit, Power and Computing Technologies (ICCPCT, Nagercoil, India, 2016.
- [16] K. Teranishi, N. Shimomura, S. Suzuki, and H. Itoh, 'Development of dielectric barrier discharge-type ozone generator constructed with piezoelectric transformers: effect of dielectric electrode materials on ozone generation', *Plasma Sources Sci. Technol.*, vol. 18, no. 4, pp. 045011-045011 (10), 2009, doi: 10.1088/0963-0252/18/4/045011.
- [17] K. Teranishi, S. Suzuki, and H. Itoh, 'Dielectric barrier discharge generated by piezoelectric transformer in atmospheric pressure', *IEEE Trans. Plasma Sci.*, vol. 33, no. 2, pp. 296–297, Apr. 2005, doi: 10.1109/TPS.2005.845081.
- [18] H. Itoh, K. Kobayashi, K. Teranishi, N. Shimomura, and S. Suzuki, 'Time-Resolved Observation of Self-Organized Filaments Formed in a Helium-Dielectric

- Barrier Discharge', *IEEE Trans. Plasma Sci.*, vol. 39, no. 11, pp. 2204–2205, Nov. 2011, doi: 10.1109/TPS.2011.2160568.
- [19] J. D. Boles, J. J. Piel, N. Elaine, J. E. Bonavia, J. H. Lang, and D. J. Perreault, 'Piezoelectric-Based Power Conversion: Recent Progress, Opportunities, and Challenges.', in *IEEE Custom Integrated Circuits Conference (CICC*, Newport Beach, CA, USA, 2022.
- [20] J. S. Kim, K. Choi, and I. Yu, 'A New Method of Determining the Equivalent Circuit Parameters of Piezoelectric Resonators and Analysis of the Piezoelectric Loading Effect', *IEEE Trans. Ultrason.* Ferroelectr. Freq. CONTROL, vol. 40, no. 4, pp. 424– 426, 1993.
- [21] J. D. Boles, J. E. Bonavia, J. H. Lang, and D. J. Perreault, 'A Piezoelectric-Resonator-Based DC-DC Converter Demonstrating 1 kW/cm Resonator Power Density', *IEEE Trans. Power Electron.*, vol. 38, no. 3, pp. 2811–2815, 2023, doi: 10.1109/TPEL.2022.3217773.
- [22] H. O'Keeffe, M. P. Foster, and J. N. Davidson, 'Parameterisation methods for piezoelectric transformer equivalent circuit models', in 11th International Conference on Power Electronics, Machines and Drives (PEMD 2022), Newcastle, UK: IET Digital Library, 2022, pp. 764–768.
- [23] H. Itoh, M. Taguchi, and S. Suzuki, 'Thermal decomposition of ozone at high temperature leading to ozone zero phenomena', *J. Phys. Appl. Phys.*, vol. 53, no. 18, p. 185206, 2020, doi: 10.1088/1361-6463/ab71a9.



Henry O'Keeffe received the M.Eng. degree in electronic and electrical engineering in 2020 and completed his PhD in power supply design for plasma chemical reactors in 2025 both at the University of Sheffield, Sheffield, U.K.

His wider research interests include resonant power supply design, DC-DC and DC-AC conversion, and multi-level converters.



Martin P. Foster received the B.Eng. degree in electronic and electrical engineering, the M.Sc.(Eng.) degree in control systems, and the Ph.D. degree from the University of Sheffield, Sheffield, U.K., in 1998, 2000, and 2003, respectively. His Ph.D. dissertation was titled "Analysis and Design of High-order Resonant Power Converters."

In 2003, he became a Member of Academic Staff specializing in power electronic systems with the University of Sheffield, where he became Senior Lecturer in 2010, Reader in 2014, and Professor of Energy Storage and Conversion in 2017. His current research interests include the modelling and control of switching power converters, resonant power supplies, multilevel converters, energy storage

management systems, piezoelectric transformers and power electronic packaging, and thermal management.



Jonathan N. Davidson received the M.Eng. degree in electronic engineering and the Ph.D. degree in thermal modelling and management from the University of Sheffield, Sheffield, U.K., in 2010 and 2015, respectively.

In 2015, he became a Lecturer in electrical engineering with the University

of Sheffield, where he was made a Senior Lecturer in 2022. His research interests include thermal modelling and management of power electronics, and the design and analysis of piezoelectric transformer-based and resonant power converters, high-voltage power supplies for plasma chemistry, and wastewater sensing systems.